

Transfer-Free Fabrication and Characterisation of Transparent Multilayer CVD Graphene MEAs for In-Vitro Optogenetic Applications

González, Gonzalo León ; Deng, Shanliang; Vollebregt, Sten; Giagka, Vasiliki

DOI

[10.1109/MeMeA60663.2024.10596734](https://doi.org/10.1109/MeMeA60663.2024.10596734)

Publication date

2024

Document Version

Final published version

Published in

Proceedings of the 2024 IEEE International Symposium on Medical Measurements and Applications (MeMeA)

Citation (APA)

González, G. L., Deng, S., Vollebregt, S., & Giagka, V. (2024). Transfer-Free Fabrication and Characterisation of Transparent Multilayer CVD Graphene MEAs for In-Vitro Optogenetic Applications. In *Proceedings of the 2024 IEEE International Symposium on Medical Measurements and Applications (MeMeA)* IEEE. <https://doi.org/10.1109/MeMeA60663.2024.10596734>

Important note

To cite this publication, please use the final published version (if applicable). Please check the document version above.

Copyright

Other than for strictly personal use, it is not permitted to download, forward or distribute the text or part of it, without the consent of the author(s) and/or copyright holder(s), unless the work is under an open content license such as Creative Commons.

Takedown policy

Please contact us and provide details if you believe this document breaches copyrights. We will remove access to the work immediately and investigate your claim.

Green Open Access added to TU Delft Institutional Repository

'You share, we take care!' - Taverne project

<https://www.openaccess.nl/en/you-share-we-take-care>

Otherwise as indicated in the copyright section: the publisher is the copyright holder of this work and the author uses the Dutch legislation to make this work public.

Transfer-free Fabrication and Characterisation of Transparent Multilayer CVD Graphene MEAs for in-vitro Optogenetic Applications

Gonzalo León González¹, Shanliang Deng^{2,3}, Sten Vollebregt², and Vasiliki Giagka^{1,4}

¹Bioelectronics Section, Department of Microelectronics, TU Delft, Delft, The Netherlands

²Electronic Components, Technology and Materials Section, Department of Microelectronics, TU Delft, Delft, The Netherlands

³Laboratory of Experimental Cardiology, Department of Cardiology, Leiden University Medical Center, Leiden, The Netherlands

⁴Technologies for Bioelectronics group, Department of System Integration and Interconnection Technologies, Fraunhofer IZM, Berlin, Germany

Abstract—This study explores the application of a novel transfer-free method for the synthesis of multilayer Chemical Vapour Deposition (CVD) graphene directly on transparent substrates, specifically to create transparent Microelectrode Arrays (MEAs) for optogenetic studies. Traditional methods typically involve a graphene transfer step that can compromise the material's integrity and electrical properties. By eliminating this step, our approach simplifies the fabrication process. The developed MEAs were characterised by Raman spectroscopy, optical transmittance, and electrochemical impedance spectroscopy. We also assessed the stability and recording capabilities of the fabricated MEAs, alongside a comparative assessment with a commercial MEA. Turbostratic graphene grown directly on quartz and sapphire was successfully achieved. Our transfer-free MEAs exhibit promising signal detection capabilities, despite a relatively high baseline noise of $\sim 23 \mu V$, and a significantly large impedance at 1 kHz (3.2 to 9.89 $M\Omega$) surpassing values in other studies. The devices exhibited low stability after exposure to liquid media during the soaking and ageing tests, causing large variations in the electrochemical measurements post-exposure. This was due to the permeability of the encapsulation layer and the biodegradability of the molybdenum structures, which led to significant structural and chemical changes in the devices. While further work is required to prevent the failure mechanisms of the device, this study demonstrates the feasibility of transparent MEA fabrication by means of a transfer-free approach directly on quartz substrates.

Index Terms—graphene, chemical vapour deposition, microelectrode array, optogenetic compatibility

I. INTRODUCTION

Graphene is a useful and versatile material for cellular interfacing due to its exceptional combination of properties, including excellent electrical and electrochemical performance, flexibility and transparency [1], [2]. It thus lends itself to applications for multimodal interactions with tissue, such as

Funding received from the Dutch Brain Interface Initiative (DBI2) and the Chips Joint Undertaking in collaboration with the European Union's Horizon Framework Programme and National Authorities (NerveRepack, Grant Agreement n° 101112347).

neural interfaces with recording and stimulating capabilities in the electrical and optical domains [1]–[3].

Among its applications, this material is particularly interesting for the creation of in-vitro platforms intended for cell interfacing, enabling the systematic study of cellular behaviour and interactions in response to various stimuli, while monitoring the cells optically and electrically [4]. Thus, fully transparent Microelectrode Arrays (MEAs) are of interest. These have traditionally been fabricated with ITO, although more recently, non-metallic materials such as graphene have also been used [1].

Graphene-based optically transparent MEAs have been previously fabricated, typically employing Chemical Vapour Deposition (CVD) graphene. However, they require an additional transfer step of the graphene onto the desired substrate [4]–[7]. This process can lead to the contamination of the sample or physical damage that will result in a decrease in the quality of graphene, thus degrading its electrical properties [8].

We have previously pioneered a transfer-free approach to fabricate multilayer CVD graphene on silicon (Si) substrates [8]. We have utilised this technique to fabricate optically transparent and MRI-compatible graphene neural electrodes on flexible substrates with excellent stimulating properties [1], [3], [9]. Furthermore, we have recently shown that further electrochemical enhancement can be achieved by locally printing Pt nanoparticles using spark ablation, without compromising the optical transparency, which is essential for optogenetic compatibility [3].

This paper explores the fabrication of transparent in-vitro MEAs using transfer-free CVD-grown multilayer graphene, directly on transparent substrates, for cardiomyocyte optogenetic research.

II. MATERIALS AND METHODS

A. Substrate Selection

Before fabricating the devices, we evaluated quartz and sapphire as potential substrates for graphene growth. We employed our transfer-free process, and varying CVD settings on both substrates to determine the optimal parameters for graphene synthesis. For the transfer-free process, a sacrificial Molybdenum (Mo) layer is deposited and patterned on the transparent substrate, and later used as the catalyst for graphene growth before being removed [8]. The samples used consisted of dies with fragments of patterned graphene MEA circuits. We assessed the graphene quality using Raman spectroscopy, employing a 514 nm laser.

Following the parameter optimisation, additional graphene samples were grown on each substrate. These samples underwent sterilisation using 100% ethanol for 20 min and a soaking test where they were sterilised in 70% ethanol for 20 min and immersed in a cell differentiation medium for 12 days [10]. The presence and integrity of graphene before and after these treatments was validated using Raman spectroscopy and Optical Microscopy (OM), respectively.

To estimate the number of graphene layers, we grew an unpatterned $15 \times 15 \text{ mm}^2$ graphene sample on the chosen substrate, quartz, using the identified optimal parameters (Section II-B). After the removal of the underlying Mo layer, an Optical Transmittance (OT) measurement was conducted across wavelengths ranging from 300 to 1200 nm at 5 nm intervals. We also measured the OT of bare quartz to serve as a reference.

B. Fabrication

In this study, we fabricated the proposed devices, with the same layout as MultiChannel Systems (MCS) 60MEA200/30iR-Ti MEAs, on a 100 mm quartz wafer using four lithography masks. The devices consisted of 59 recording electrodes with a $30 \mu\text{m}$ diameter and a larger return electrode further away from the rest. Initially, a 50 nm Mo layer was sputtered onto the wafer, serving as a catalyst for graphene growth. This Mo layer was patterned via photolithography and plasma etching. Subsequently, graphene was synthesised on the patterned Mo through CVD (AIXTRON Black Magic Pro) at around 915°C with 960, 40, and 25 sccm of Ar, H_2 , and CH_4 gas flows, respectively, at 25 mbar pressure for 20 min (Fig. 1a) [1].

Next, we sputtered a layer of pure aluminium (pAl), using titanium (Ti) as an adhesion layer. This layer was patterned through photolithography and wet etching to form protective landing pads over the graphene electrodes (Fig. 1b). This step safeguards the electrodes while creating openings in the encapsulation layer in a subsequent stage (Fig. 1e).

To fabricate the device's metal tracks and contact pads, a layer of 200 nm Au with a 10 nm Ti adhesion layer was deposited via physical vapour deposition. The Au was patterned through liftoff (Fig. 1c). These structures connect the graphene electrodes to the recording apparatus.

Following this, we encapsulated the front side of the device in $1 \mu\text{m}$ of Parylene C (Fig. 1d). Openings were then created

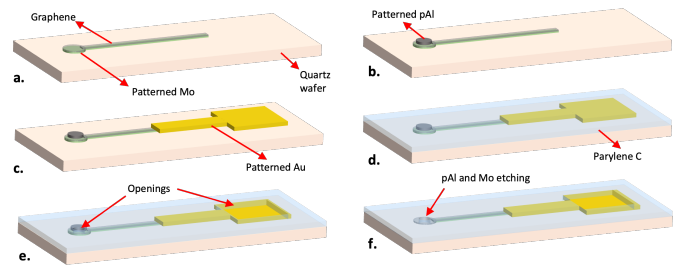


Fig. 1. Microfabrication process flow. (a) Graphene growth on patterned Mo. (b) Protective pAl landing pad above graphene electrodes. (c) Au tracks and contact pads. (d) Encapsulation with parylene C. (e) Electrode and contact pad openings created through oxygen plasma. (f) Etch of pAl landing pads and Mo beneath the electrodes.

using oxygen plasma and a photoresist mask created through photolithography (Fig. 1e). The devices were diced, and the pAl pads, along with the Mo beneath the graphene electrodes (excluding the tracks), were etched using a 0.55% HF solution, and a 37% H_2O_2 solution (Fig. 1f), respectively. Subsequently, the presence of graphene on the electrodes was confirmed through Raman spectroscopy.

Finally, the graphene microelectrode arrays (gMEAs) were assembled. They were affixed to a PCB and connected through Au ball wire bonding. A culture medium well was then centrally attached to the MEA (Fig. 2UL). The samples were named with a conventional approach based on their characteristics and fabrication batch.

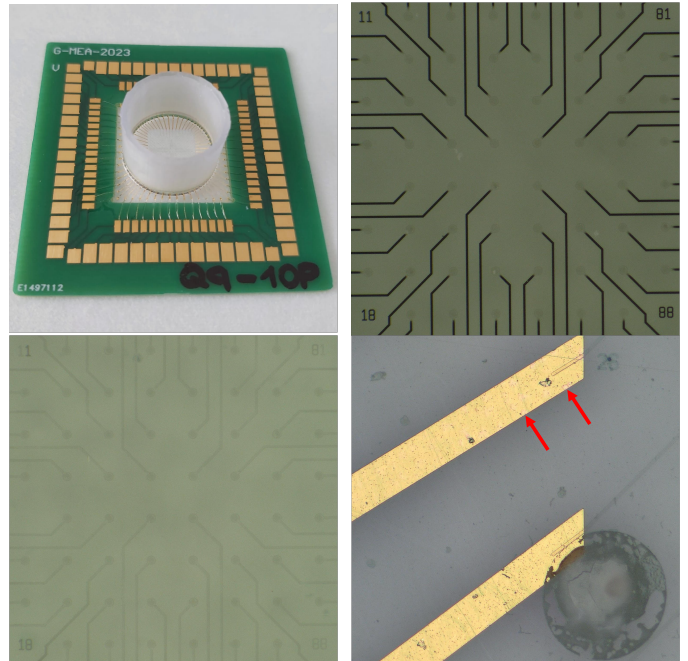


Fig. 2. Upper left: Fabricated MEA attached and wire bonded to an adaptor PCB, with a growing well. Upper right: Microscope image of the fabricated MEA electrodes. Lower left: Microscope image of MEA electrodes after soaking test. Lower right: Defects after ageing test. Visible PBS salt deposit, and indicated with arrows some crystallised Mo compounds above Au track.

C. Device Characterisation

After fabrication, the device's signal-to-noise ratio (SNR) was evaluated. For these tests, we utilised an amplifier (MCS, FM60-AMP Rev.B SerNo. 047), with the devices mounted in it, and containing Phosphate Buffered Saline (PBS) in the growing well. A platinum electrode, positioned at the edge of the well, delivered various waveforms (sine, square, no-stimulation) at different voltage amplitudes (1V, 100mV, and 10mV) into the PBS.

The baseline noise was determined as the Root Mean Square (RMS) of recordings without stimulation. Similarly, the signal level of sinusoidal stimulations was calculated as the RMS of the entire recording. For square stimulations, only the RMS of segments during stimulation were considered, averaging their values to determine the signal level. The SNR was calculated as the signal level divided by the baseline noise for each electrode independently, excluding damaged or unstable electrodes [13].

Finally, the devices were soaked in a cell culture medium as detailed earlier (II-A), to study the environment's effects. Post-soaking, we reassessed the SNR. Concurrently, some devices were allocated for an accelerated ageing test to investigate long-term stability. This test involved incubating the devices in PBS at 67°C for 10 days [11]. We conducted electrochemical impedance spectroscopy (EIS) measurements on these devices before and periodically during the ageing test. EIS was performed in PBS with a three-electrode setup, using a Pt and Ag/AgCl electrode as the counter and reference electrode, respectively [1]. OT measurements were taken before and after each procedure in both the soaking and ageing tests.

III. RESULTS AND DISCUSSION

A. Graphene Characterisation

All Raman spectra of the graphene samples produced using various CVD parameters exhibited I_{2D}/I_G ratios, defined as the intensity of the 2D peak relative to the G peak, that were < 1 , and the Full Width at Half Maximum (FWHM) of the 2D peaks $\sim 75\text{cm}^{-1}$, indicating the formation of multilayer graphene. Additionally, the fitting of the 2D peaks was achieved by a single Lorentzian, suggesting turbostratic graphene was produced. The optimum parameters were selected based on the smallest I_D/I_G ratios, which compare the intensity of the D peak to that of the G peak. These ratios reflect the quality of graphene and were 0.52 for quartz and 0.3 for sapphire. This criterion was paired with the requirement for minimal noise in the Raman spectra [1], [9], [14], [15].

Using Raman spectroscopy, we confirmed the existence of graphene on the substrates through the identification of the three characteristic graphene peaks in the spectra: the D, G, and 2D peaks. Subsequently we evaluated the graphene structures' integrity after the various procedures using OM. It was observed that the most detrimental process to the graphene integrity was the removal of Mo, often leading to delamination due to the lack of supporting structures. In contrast, neither the ethanol sterilisation nor the soaking tests exhibited significant

adverse effects on the graphene. Consequently, quartz was chosen as the preferred substrate, based on its resilience to delamination post-Mo removal and its lower cost compared to sapphire.

Lastly, using the OT measurement at 550 nm, it was estimated that approximately 10 layers of graphene had been grown through the CVD process on quartz [12].

B. Initial Device Characterisation

Upon completion of the MEAs, the presence of graphene on the electrodes was verified using Raman spectroscopy.

The initial characterisation of the gMEAs revealed a baseline noise of $\sim 23 \mu\text{V}$ [Tbl. I]. While this noise level enabled the detection of larger amplitude stimulations at 1 V, it hindered and overwhelmed those at 100 mV and 10 mV, respectively [Tbl. II and III]. A notable variation in RMS, and corresponding SNR, was observed across different devices and their electrodes. This was attributed to fabrication defects such as inhomogeneities in CVD-grown graphene and structural damage. Further examination through EIS showed an impedance at 1 kHz ranging from 3.2 to 9.89 $M\Omega$ [Tbl. IV], substantially higher than in other studies [1], [3], [5]–[7]. However, when area normalised, the impedance remained comparable to reported values.

Additionally, an assessment of the signals in the form of a normalised power spectrum revealed the presence of a significant 50 Hz peak attributed to the power line noise.

C. Soaking test

The OT measurements taken before and after the soaking tests generally indicated increased transmittance across all monitored wavelengths. This finding was corroborated by OM, which showed significant removal of the Mo layer beneath the graphene tracks during the soaking test. Remarkably, this Mo removal extended to areas not directly exposed through openings in the parylene C, suggesting the material's permeability to the culture medium (Fig. 2 UR and LL).

Post-soak test, the devices remained capable of recording signals, although with notable variations in baseline noise and sensitivity. The baseline noise decreased to an average of $\sim 10 \mu\text{V}$ [Tbl. I], while recorded signal amplitudes decreased by $\sim 50\%$ on average [Tbl. II and III], indicating an altered device sensitivity. Furthermore, an increase in the Standard Deviation (SD) of the signal RMS and corresponding SNR, with respect to the initial SDs, indicates greater differences among electrodes. These changes arise from the permeability of the encapsulation layer and the degradation of Mo, which alter the electrochemical properties of the circuit.

D. Ageing Test

OT measurements increased during the ageing test, starting from day 2 and peaking on day 10 [Fig. 3]. This trend, similar to that observed during the soaking test, is attributed to the degradation of the opaque Mo layer due to the encapsulation layer's permeability to PBS. Additional examination of the devices using OM confirmed the deterioration of Mo and

revealed the presence of other defects, including salt deposits beneath the encapsulation layer [Fig. 2 (LR)], and parylene C delamination above Au structures on days 1 and 4, respectively.

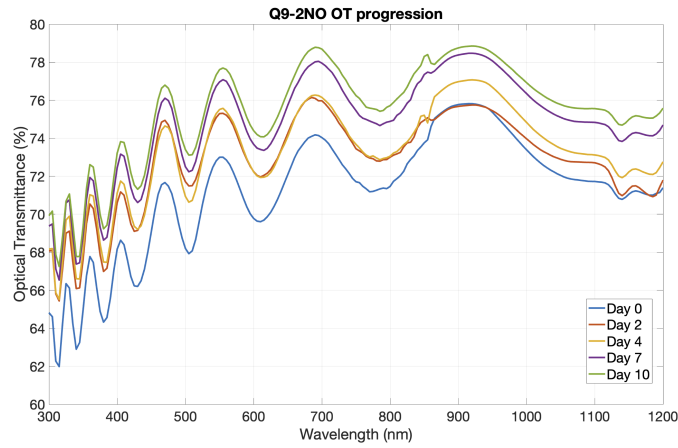


Fig. 3. Progression of device Q9-2NO's optical transmittance during the ageing test.

Similarly, EIS measurements revealed behavioural variations in the devices. The most significant changes occurred within the first few days, stabilising the latest by day 4. We observed a dramatic reduction in impedance across all frequencies during this period, showing a drop of up to 99% between the initial and final measurements at 1kHz of some samples [Tbl. IV and Fig. 4].

Devices	Noise RMS [μV]		
	Run 1	Run 2	Run 3
Q9-2OP	17.04 \pm 2.88 (Av. 54)	7.73 \pm 2.02 (Av.52)	9.2 \pm 3.4 (Av. 51)
Q9-3OP	36.93 \pm 12.76 (Av. 45)	8.01 \pm 2.39 (Av.49)	9.92 \pm 5.88 (Av. 50)
Q9-4OP	18.16 \pm 4.16 (Av. 46)	9.42 \pm 2.59 (Av.48)	
QN-2	26.57 \pm 9.21 (Av. 20)	11.49 \pm 4.5 (Av.53)	12.48 \pm 3.45 (Av.45)
QN-3		16.2 \pm 8.23 (Av. 36)	11.82 \pm 4.64 (Av.42)
QN-4		22.97 \pm 11.92 (Av. 27)	68.83 \pm 32.41 (Av.29)

MCS1	4.33 \pm 5.4 (Av.54)
MCS2	3.96 \pm 3.5 (Av.52)
MCS3	3.69 \pm 2.2 (Av.46)

TABLE I

RMS OF BASELINE NOISE OF THE TESTED DEVICES. COLOUR CELLS INDICATE MEASUREMENT WAS TAKEN AFTER: 2-DAY (GREEN), 4-DAY (PINK), AND 12-DAY (BLUE) SOAK TESTS, OR WHITE IF NO TREATMENT WAS APPLIED. EVERY CELL PROVIDES THE RMS OF THE BASELINE NOISE IN THE FORM [AVERAGE \pm SD (NUMBER OF ELECTRODES USED FOR THE AVERAGE AND SD)]. MCS 1-3 ARE THE MULTICHANNEL SYSTEMS MEAS.

There was also a noticeable shift in phase. The Bode plot's phase angle initially indicated a largely capacitive behaviour, continuing to rise beyond -90° at frequencies above 10^4 Hz

(suggesting non-ideal capacitive behaviour). This behaviour shifted over time, showing capacitive characteristics at low frequencies up to 10^1 Hz, transitioning to more resistive behaviour up to 10^4 Hz, and then rapidly rising to a mostly capacitive behaviour by 10^5 Hz [Fig. 5].

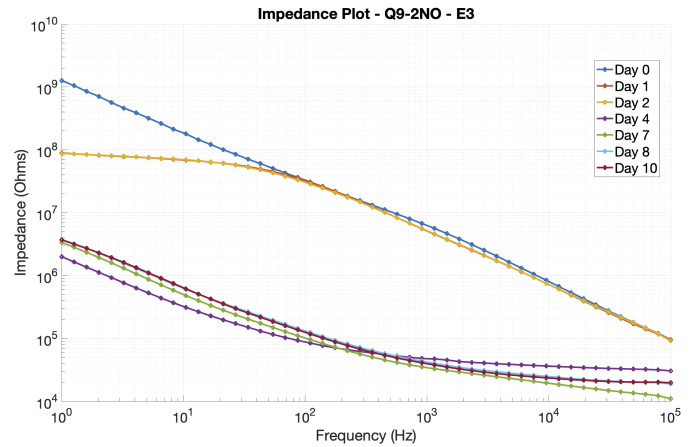


Fig. 4. Impedance Bode plot progression of device Q9-2NO, electrode 3 during ageing test.

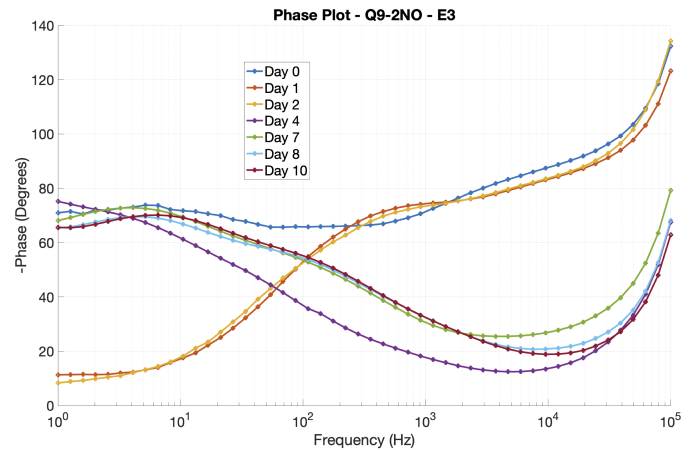


Fig. 5. Phase Bode plot progression of device Q9-2NO, electrode 3 during ageing test.

The infiltration of fluid and degradation of the Mo layer are the primary contributors to the changes observed in EIS measurements, resulting in short circuits that lower the overall resistance of the device and lead to a decreased impedance. Similarly, introducing conductive paths due to PBS infiltration can result in a more resistive behaviour, causing a reduction in the phase angles as the capacitive elements are bypassed.

E. Benchmark

The commercial MCS 60MEA200/30iR-Ti MEAs (MCS-MEAs) were assessed and compared to our devices based on their SNR, using the gMEAs' initial characterisation values. As expected, the highest SNRs were achieved during the 1 V stimulation and decreased exponentially with decreasing stimulation amplitude. The MCS-MEA outperformed the gMEA

Signal RMS (sine) [μV]									
Devices	Run 1			Run 2			Run 3		
	1 V	100 mV	10 mV	1 V	100 mV	10 mV	1 V	100 mV	10 mV
Q9-2OP	1257.32± 179.48 (Av. 54)	40.94± 9.93 (Av.54)	19.01± 5.87 (Av.54)	196.11± 127.68 (Av.52)	13.96± 5.31 (Av.52)	8.22± 2.26 (Av.52)	435.28± 142.73 (Av.51)	15.18± 4.45 (Av.51)	7.97± 2.58 (Av.51)
Q9-3OP	310.01± 128.36 (Av. 45)	32.33± 5.57 (Av.45)	18.19± 3.32 (Av.45)	383.25± 424.43 (Av.49)	26.52± 31.63 (Av.49)	9.22± 2.9 (Av.49)	494.15± 385.41 (Av.50)	22.64± 26.41 (Av.50)	8.91± 2.86 (Av.50)
Q9-4OP	1134.14± 202.45 (Av.46)	41.8± 9.16 (Av.46)	19.51± 4.28 (Av.46)	127.57± 32.38 (Av.48)	12.29± 3.39 (Av.48)	10.86± 2.99 (Av.48)			
QN-2	1149.49± 310.1 (Av.20)	58.35± 22.49 (Av.20)	23.14± 4.91 (Av.20)	426.92± 409.43 (Av.53)	29.38± 36.2 (Av.52)	11.83± 4.13 (Av.53)	513.37± 270.26 (Av.45)	15.32± 8.08 (Av.45)	13.97± 5.75 (Av.45)
QN-3				366.58± 283.63 (Av.36)	21.0± 13.2 (Av.36)	14.78± 7.45 (Av.36)	523.98± 291.0 (Av.42)	16.22± 6.65 (Av.42)	11.98± 4.53 (Av.42)
QN-4				554.34± 472.08 (Av.27)	41.43± 28.28 (Av.27)	22.1± 12.19 (Av.27)	476.08± 203.87 (Av.29)	75.85± 34.98 (Av.29)	74.07± 35.12 (Av.29)
	1 V			100 mV			10 mV		
MCS1	461.1±344.41 (Av.54)			16.9±13.48 (Av.54)			3.14±1.28 (Av.54)		
MCS2	500.66±356.89 (Av.52)			19.16±17.67 (Av.52)			3.52±1.89 (Av.52)		
MCS3	387.28±241.61 (Av.46)			15.6±9.3 (Av.46)			3.23±0.93 (Av.46)		

TABLE II

RMS OF THE SIGNAL OF THE TESTED DEVICES FROM SINUSOIDAL WAVEFORM STIMULATION. COLOUR CELLS INDICATE MEASUREMENT WAS TAKEN AFTER: 2-DAY (GREEN), 4-DAY (PINK), AND 12-DAY (BLUE) SOAK TESTS, OR WHITE IF NO TREATMENT WAS APPLIED. EVERY CELL PROVIDES THE RMS OF THE SIGNAL IN THE FORM [AVERAGE±SD (NUMBER OF ELECTRODES USED FOR THE AVERAGE AND SD)]. MCS 1-3 ARE THE MULTICHANNEL SYSTEMS MEAS.

Signal RMS (square) [μV]									
Devices	Run 1			Run 2			Run 3		
	1 V	100 mV	10 mV	1 V	100 mV	10 mV	1 V	100 mV	10 mV
Q9-2OP	517.28± 52.21 (Av. 54)	69.16± 17.64 (Av.54)		225.85± 61.15 (Av.52)	27.02± 16.06 (Av.52)	7.44± 1.96 (Av.52)	326.49± 54.93 (Av.51)	20.46± 6.37 (Av.51)	8.76± 2.54 (Av.51)
Q9-3OP	246.41± 99.01 (Av.45)	42.43± 12.5 (Av.45)	18.62± 3.83 (Av.45)	209.55± 188.8 (Av.49)	27.13± 23.96 (Av.49)	15.16± 17.82 (Av.49)	393.73± 160.05 (Av.50)	55.68± 56.14 (Av.50)	8.18± 2.62 (Av.50)
Q9-4OP	642.54± 60.8 (Av.46)	80.12± 14.98 (Av.46)	18.93± 3.84 (Av.46)	242.25± 85.2 (Av.48)	21.39± 6.52 (Av.48)	9.37± 2.83 (Av.48)			
QN-2	744.73± 142.34 (Av.20)	84.09± 27.38 (Av.20)	27.47± 4.84 (Av.20)	409.37± 194.75 (Av.53)	27.53± 20.51 (Av.53)	11.63± 4.63 (Av.53)	417.26± 134.88 (Av.45)	33.94± 23.4 (Av.45)	15.3± 6.15 (Av.45)
QN-3				393.44± 138.06 (Av.36)	30.32± 22.11 (Av.36)	12.56± 5.49 (Av.36)	352.03± 91.49 (Av.42)	13.8± 4.72 (Av.42)	12.69± 4.88 (Av.42)
QN-4				280.66± 200.24 (Av.27)	60.05± 38.76 (Av.27)	21.39± 10.24 (Av.27)	462.24± 117.59 (Av.29)	81.83± 38.67 (Av.29)	73.67± 34.93 (Av.29)
	1 V			100 mV			10 mV		
MCS1	414.16±197.89 (Av.54)			10.02±9.72 (Av.54)			4.05±1.98 (Av.54)		
MCS2	393.85±199.17 (Av.52)			20.67±21.44 (Av.52)			6.27±4.68 (Av.52)		
MCS3	403.83±154.78 (Av.46)			10.83±6.16 (Av.46)			2.84±0.58 (Av.46)		

TABLE III

RMS OF THE SIGNAL OF THE TESTED DEVICES FROM SQUARE WAVEFORM STIMULATION. COLOUR CELLS INDICATE MEASUREMENT WAS TAKEN AFTER: 2-DAY (GREEN), 4-DAY (PINK), AND 12-DAY (BLUE) SOAK TESTS, OR WHITE IF NO TREATMENT WAS APPLIED. EVERY CELL PROVIDES THE RMS OF THE SIGNAL IN THE FORM [AVERAGE±SD (NUMBER OF ELECTRODES USED FOR THE AVERAGE AND SD)]. MCS 1-3 ARE THE MULTICHANNEL SYSTEMS MEAS.

TABLE IV

EVOLUTION OF AVERAGE IMPEDANCE AT 1KHZ AND AREA NORMALISED IMPEDANCE DURING AGEING TEST. THE NUMBER OF ELECTRODES USED TO CALCULATE THE AVERAGE AND SURFACE AREA OF ELECTRODES IS NOTED NEXT TO THE DEVICE NAME. THE DIFFERENCES IN SURFACE AREA ARE DUE TO THE ELECTRODE OPENINGS ON SOME DEVICES.

Device		Day						
		0	1	2	4	7	8	10
Q9-2NO (av. 16)	Impedance ($10^4\Omega$)	522.94 ± 311.2	560.14 ± 220.41	519.99 ± 178.21	4.23 ± 1.51	4.05 ± 1.92	4.10 ± 1.73	4.67 ± 1.31
	Area Normalised Impedance (Ωcm^2)	36.96 ± 22.0	39.59 ± 15.58	36.76 ± 12.6	0.3 ± 0.11	0.29 ± 0.14	0.29 ± 0.12	0.33 ± 0.09
	Area: $\sim 707 \mu m^2$							
Q9-4OP (av. 15)	Impedance ($10^4\Omega$)	320.34 ± 163.32	12.6 ± 9.36	6.68 ± 4.69	5.65 ± 3.61	7.17 ± 2.88	5.43 ± 1.73	4.85 ± 2.49
	Area Normalised Impedance (Ωcm^2)	21.11 ± 10.76	0.83 ± 0.62	0.44 ± 0.31	0.37 ± 0.24	0.47 ± 0.19	0.36 ± 0.11	0.32 ± 0.16
	Area: $\sim 659 \mu m^2$							
QN-1 (av. 11)	Impedance ($10^4\Omega$)	989.0 ± 894.8	435.0 ± 232.3	656.0 ± 332.35	547.68 ± 291.26	380.2 ± 279.54	369.98 ± 234.67	323.97 ± 218.77
	Area Normalised Impedance (Ωcm^2)	69.91 ± 63.25	30.75 ± 16.42	46.37 ± 23.49	38.71 ± 20.59	26.87 ± 19.76	26.15 ± 16.59	22.9 ± 15.46
	Area: $\sim 707 \mu m^2$							

for 1 V and 100 mV stimulations but exhibited similar values for the 10 mV stimulation, where SNR was insufficient for adequate signal detection. However, by looking at the noise and signal RMS independently, we find that the baseline noise is the main reason for the substantially lower SNR in our devices. For the MCS devices, the average baseline noise is 4 μV , compared to 23 μV observed in gMEAs [Tbl. I]. On the other hand, gMEAs attain a higher signal RMS at 1 V and 100 mV stimulations compared to MCS-MEAs [Tbl. II and III].

Additionally, we assessed the signals as normalised power spectra, revealing a negligible influence of the power line noise (50 Hz peak) on the devices.

IV. CONCLUSIONS

In this study, we fabricated and characterised transparent graphene MEAs using a transfer-free method. Our research successfully grew graphene on quartz and sapphire, diverging from previous studies utilising this transfer-free process on thermally oxidised silicon. The devices underwent comprehensive characterisation through Raman spectroscopy, OT, SNR, and EIS.

The gMEAs were effective in detecting signals at both 1 V and 100 mV stimulations, achieving satisfactory SNR for 1 V and an average SNR > 1 for 100 mV stimulations. When compared to gMEAs, the commercially available MCS-MEAs achieved similar detection ranges but with lower baseline noise and decreased signal detection levels for the same stimulations. Furthermore, MCS-MEAs were not affected by power line noise, in contrast to gMEAs, which showed significant sensitivity. EIS revealed higher impedance values for gMEAs at 1 kHz, ranging from 3.2 to 9.89 M Ω , potentially attributed to lower graphene quality or Mo degradation near the electrode.

Our investigation revealed instability in the devices during soaking in the culture medium and accelerated ageing in PBS at 67°C. This instability was attributed to the permeability of

the encapsulation layer and the biodegradability of the Mo layer beneath the graphene.

V. FUTURE WORK

Future work should focus on exploring alternative encapsulation materials or employing a thicker parylene C layer, alongside the complete removal of the Mo catalyst layer, to prevent the failure mechanisms observed in this investigation. Validation of the gMEA can be achieved through optogenetic cardiomyocyte experiments to assess biocompatibility and sensing capabilities. Additionally, we recommend refining the graphene growth recipe for quartz using the transfer-free approach, aimed at producing high-quality graphene.

ACKNOWLEDGMENT

We acknowledge Gandhika K. Wardhana, the staff of Else Kooi Laboratory and the Bioelectronics group from TU Delft University of Technology for their support and guidance throughout the project. Additionally, we acknowledge the staff of the Laboratory of Experimental Cardiology from Leiden University Medical Center for performing the soaking tests and providing the equipment for the SNR measurements.

REFERENCES

- [1] N. Bakhshae Babaroud, et al., "Multilayer CVD graphene electrodes using a transfer-free process for the next generation of optically transparent and MRI-compatible neural interfaces", *Microsyst. Nanoeng.*, vol. 8, no. 107, pp. 1-14, 2022. doi: 10.1038/s41378-022-00430-x.
- [2] K. Kostarelos et al., "Graphene in the Design and Engineering of Next-Generation Neural Interfaces", *Adv. Mater.*, vol. 29, no. 42, 2017.
- [3] N. Bakhshae Babaroud, et al., "Surface modification of multilayer graphene electrodes by local printing of platinum nanoparticles using spark ablation for neural interfacing", *Nanoscale*, vol. 16, no. 7, pp. 3549-3559, Jan. 2024. doi: 10.1039/D3NR05523J..
- [4] S. Rastogi, et al., "Graphene Microelectrode Arrays for Electrical and Optical Measurements of Human Stem Cell-Derived Cardiomyocytes", *Cel. Mol. Bioeng.*, vol. 11, no. 5, pp. 407-418, 2018.
- [5] V.Pereira Gomes et al., "Maskless production of neural-recording graphene microelectrode arrays", *J. Vac. Sci. Technol. B*, vol. 37, no. 2, 2019.
- [6] D.Kireev et al., "Versatile Flexible Graphene Multielectrode Arrays", *Biosensors*, vol. 7, no. 1, 2017.
- [7] X. Du et al., "Graphene microelectrode arrays for neural activity detection", *J Biol Phys*, vol. 41, no. 4, pp. 339-347, 2015.
- [8] S.Vollebregt et al., "A transfer-free wafer-scale CVD graphene fabrication process for MEMS/NEMS sensors", in *Proc. IEEE MEMS 2016*, Shanghai, China, 2016, pp. 17-20.
- [9] A. I. Velea, et al., "Wafer-Scale Graphene-Based Soft Electrode Array with Optogenetic Compatibility", in *Proc. IEEE MEMS 2020*, Vancouver, BC, Canada, 2020, pp. 421-424. doi: 10.1109/MEMS46641.2020.9056367
- [10] Harlaar N. et al., "Conditional immortalization of human atrial myocytes for the generation of in vitro models of atrial fibrillation". *Nat Biomed Eng.* vol. 6, no. 4, pp. 389-402, 2022.
- [11] D. Ding et al., "Evaluation of Durability of Transparent Graphene Electrodes Fabricated on Different Flexible Substrates for Chronic In Vivo Experiments", in *IEEE Transactions on Biomedical Engineering*, vol. 67, no. 11, pp. 3203-3210, 2020.
- [12] Shou-En Zhu et al., "Optical transmittance of multilayer graphene", *EPL*, vol. 108, no. 1, 2014.
- [13] S. Rastegar, et al., "Measurement of Signal-to-Noise Ratio In Graphene-based Passive Microelectrode Arrays", *Electroanalysis*, vol. 31, no. 6, pp. 991-1001, 2019.
- [14] B. Tang, et al., "Raman Spectroscopic Characterization of Graphene", *Applied Spectroscopy Reviews*, vol. 45, no. 5, pp. 369-407, 2010.
- [15] J. Garlow, et al., "Large-Area Growth of Turbostratic Graphene on Ni(111) via Physical Vapor Deposition", *Sci Rep*, vol. 6, no. 1, 2016.